Christopher Tsai
March 8, 2007
EE 355 – Imaging Radar and Its Applications

Problem Set IX
Interferometric Digital Elevation Models and Geocoding

Problem #1 – Four-Look Interferogram

After reading 1536 azimuth lines of 1280 range samples each, we employ Matlab's `angle` function to extract the interferogram phase and display it as a resampled high-resolution interferometric fringe pattern:

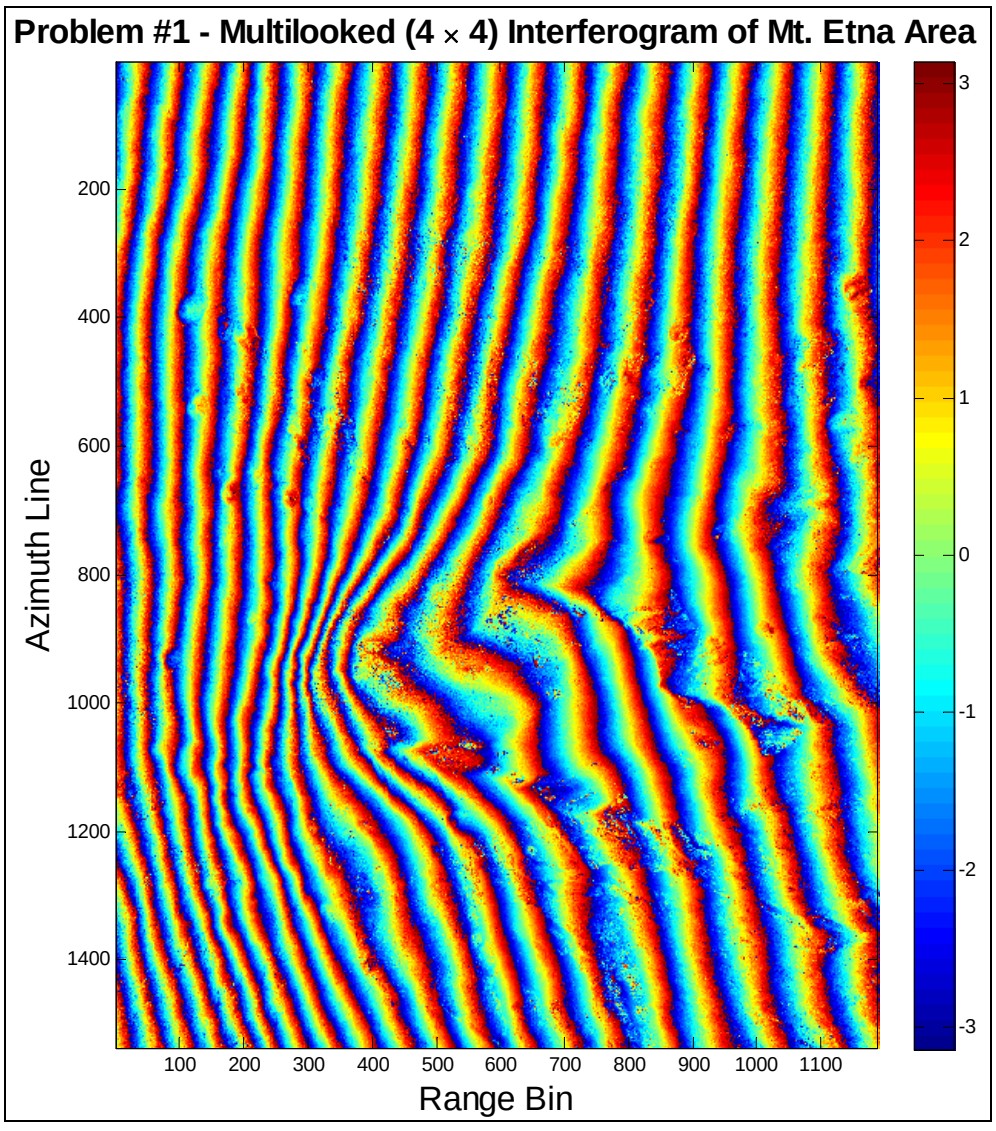

As we remarked in Problem Set VIII, this fringe pattern features high resolution from resampling and interpolation, with well-defined edges and point-like precision. The stripes (or fringes) of constant phase clearly bear 2π periodic wraparound, cycling from $-\pi$ to π. At this point, we cannot readily deduce height from the image.

Problem #2 – The Flat Earth Fringe Pattern

In general, we can relate topographical height and range by the relationship:

$$\phi = \frac{4\pi}{\lambda} B \left[\sqrt{1 - \frac{z^2}{r^2}} \cdot \cos\alpha - \frac{z}{r} \cdot \sin\alpha \right]$$

In the flat earth approximation, phase varies only along the range *r*, which we increment from r_0 by four times the slant range pixel spacing to account for the fact that each averaged resolution cell of our four-look image comprises four pixels along range. We evaluate the phase for all *r* beginning at r_0 and assuming $z = z_0$ for a flat earth. The resulting phase displays as a series of azimuth-independent fringes repeating regularly across range:

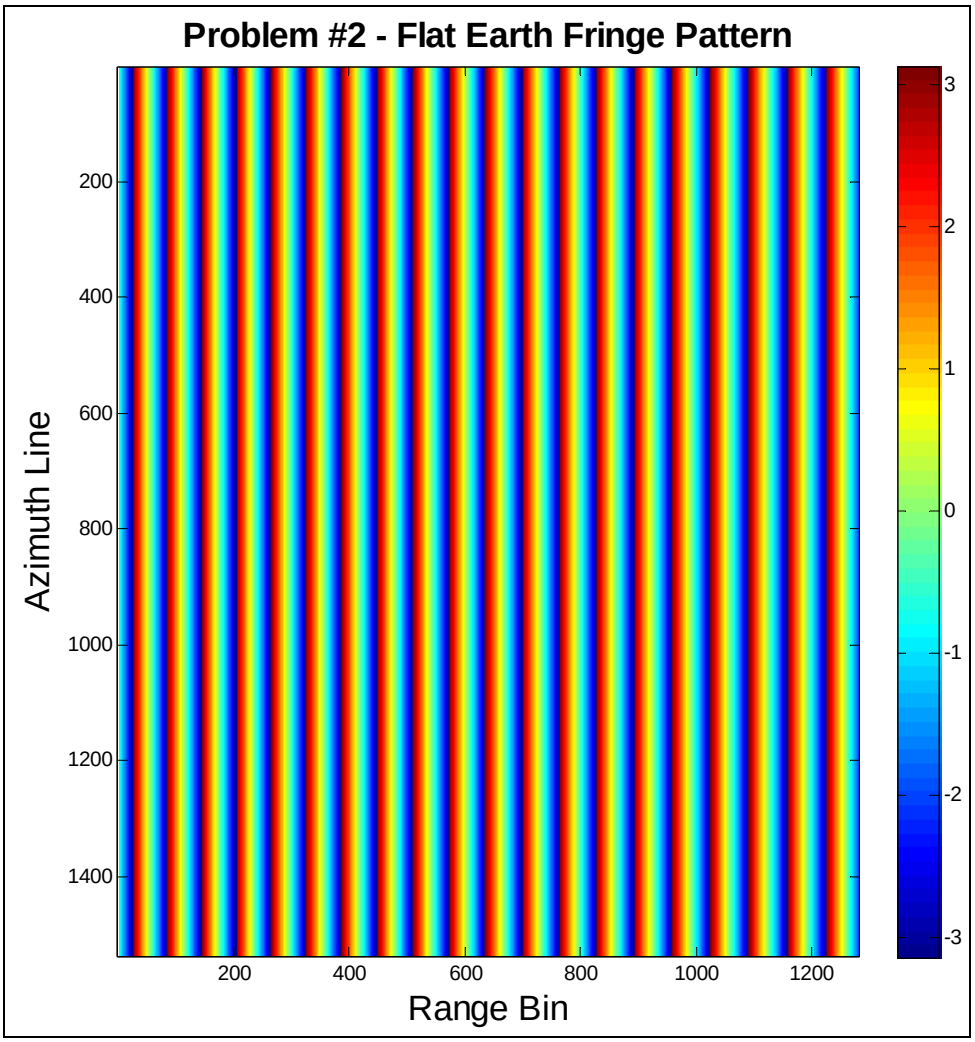

However, in the curved earth calculation, the altitude z no longer remains constant along the azimuth, since the satellite's approximately circular motion varies the effective height above ground:

$$z(t) = z_0 - \frac{1}{2}\frac{v^2 t^2}{R_{Earth} + z_0}$$

where z_0 represents the nominal spacecraft altitude, t is the azimuth time coordinate, which we increment by $\frac{4 \text{ looks}}{\text{PRF}}$ from line to line, and v is the spacecraft velocity, which we can easily compute from the effective velocity to be $v = v_{eff} \cdot \sqrt{\frac{R_{Earth}}{R_{Earth}+z}} \approx 7523.753 \frac{\text{m}}{sec}$. However, because the spacecraft moves so fast and samples at such a high pulse repetition frequency (PRF = 1736 Hz), the additional curvature that we introduce by varying the effective height actually does not noticeably change the fringe pattern that we remove from our interferogram. While the phase does vary slightly along the azimuth, the changes appear visually as only a slight slant in fringe stripes:

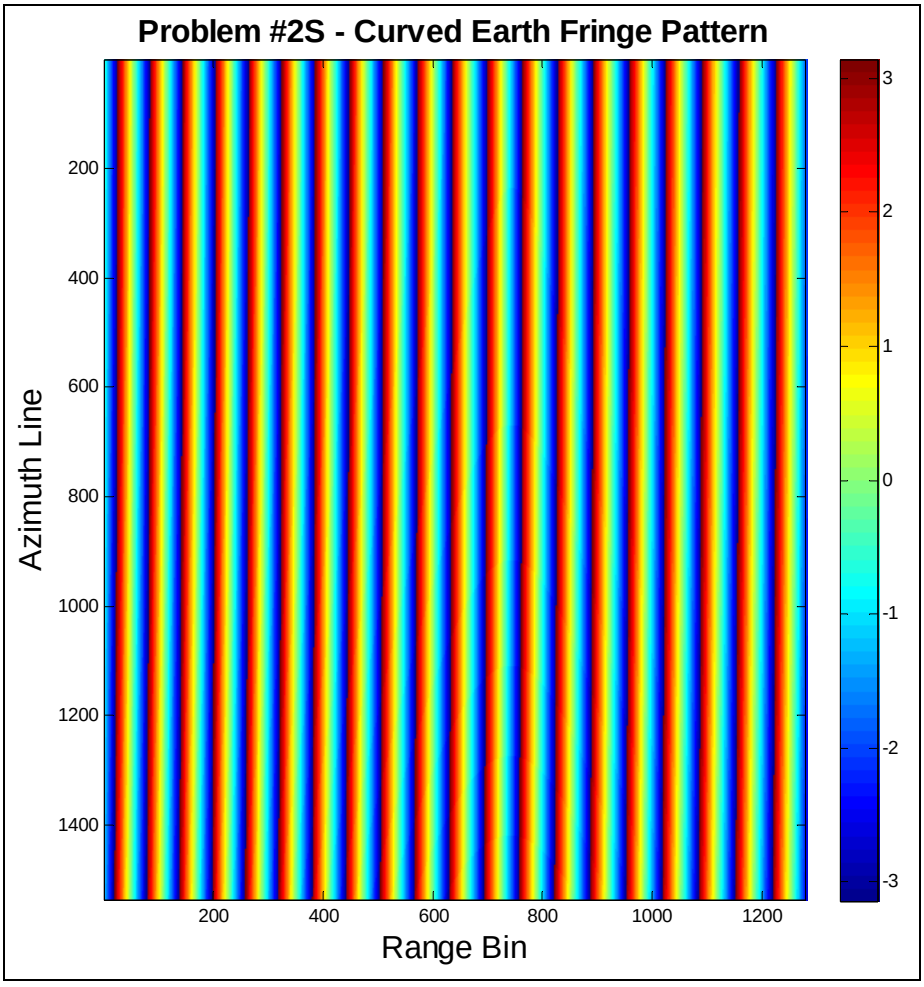

Notice that the fringes appear slightly offset to the left as we move down a single stripe from top to bottom. The curvature is most prominent along the edges of the image, farthest from our reference range bin.

Problem #3 – Removal of the Flat Earth Fringe Pattern

Flat Earth Fringe Pattern: $\phi = \frac{4\pi}{\lambda} B \left[\sqrt{1 - \frac{z^2}{r^2}} \cdot \cos\alpha - \frac{z}{r} \cdot \sin\alpha \right]$

In order to remove this phase from our original interferogram, we can simply subtract it from the `angle` result that we previously displayed as an image. However, because this phase subtraction will bring our interferogram data values out of the domain $[-\pi, \pi]$, we choose instead to modulate the interferogram with a complex correction exponential containing the *conjugate* phase of the flat earth fringe pattern *before* applying `angle`:

$$\phi_{conj} = -\frac{4\pi}{\lambda} B \left[\sqrt{1 - \frac{z^2}{r^2}} \cdot \cos\alpha - \frac{z}{r} \cdot \sin\alpha \right]$$

$$e^{j \cdot \phi_{conj}} = e^{-j \cdot \frac{4\pi}{\lambda} B \left[\sqrt{1 - \frac{z^2}{r^2}} \cdot \cos\alpha - \frac{z}{r} \cdot \sin\alpha \right]}$$

Once we remove this phase from our interferogram, our fringes begin to resemble contour lines of elevation:

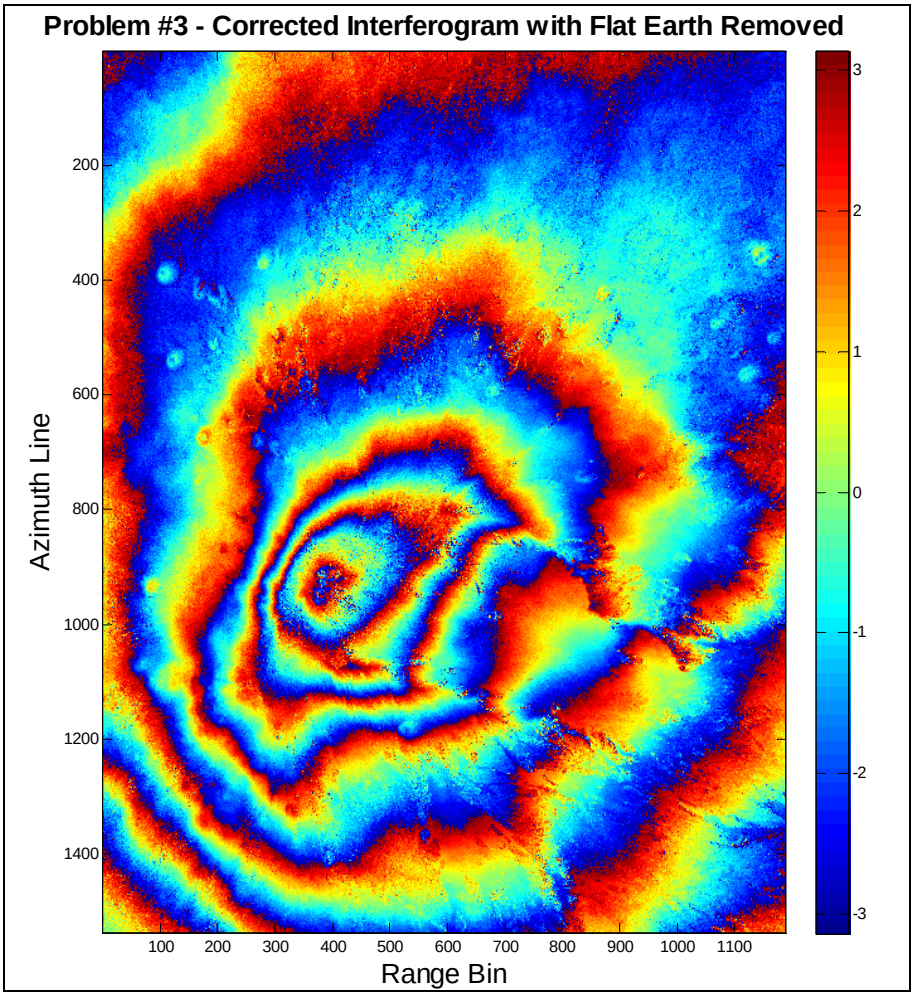

Even though the phase periodicity prevents us from immediately extracting true elevation from this interferogram, we can tell that fringes of constant phase represent lines of constant elevation, as the circular pattern resembles a gradual ascent from the peripheral flat terrain to the central peak of Mt. Etna.

Interestingly, this corrected interferogram depends quite sensitively on the orientation angle α,

$$\alpha = tan^{-1}\frac{B_{\perp}}{B_{\parallel}} + \theta_{ref} - 90° \approx -135.0462°.$$

However, if we instead employ the given value (α = -135.0°), then the fringe pattern changes slightly:

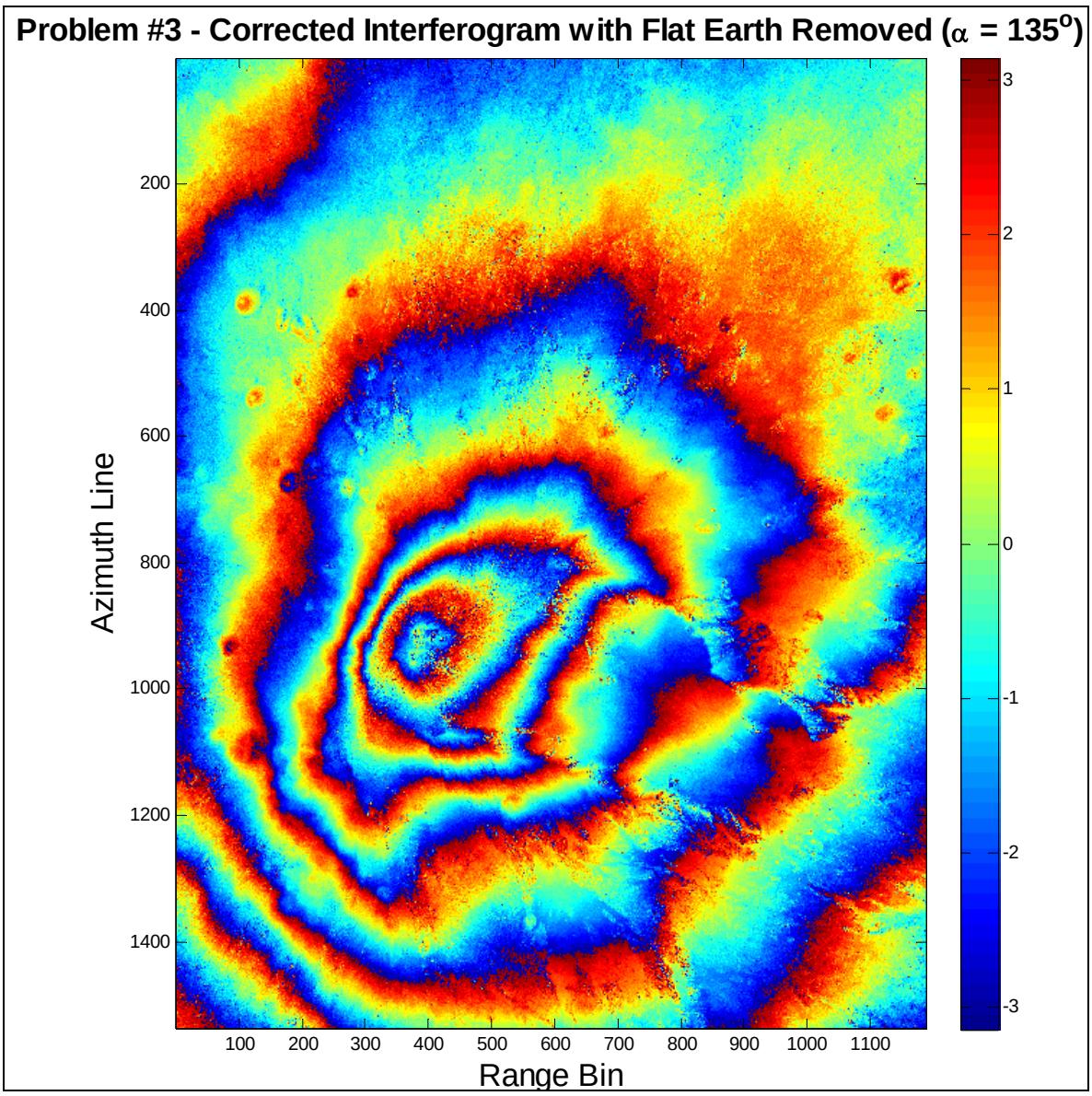

The shape of the fringe pattern surrounding Mt. Etna has metamorphosed, with a particularly more prominent ridge line in the lower right of the summit. The color (phase history) has also slightly shifted.

Removing the *curved* earth fringe pattern from the original interferogram yields an image that looks nearly identical to the fringe pattern with flat earth removed:

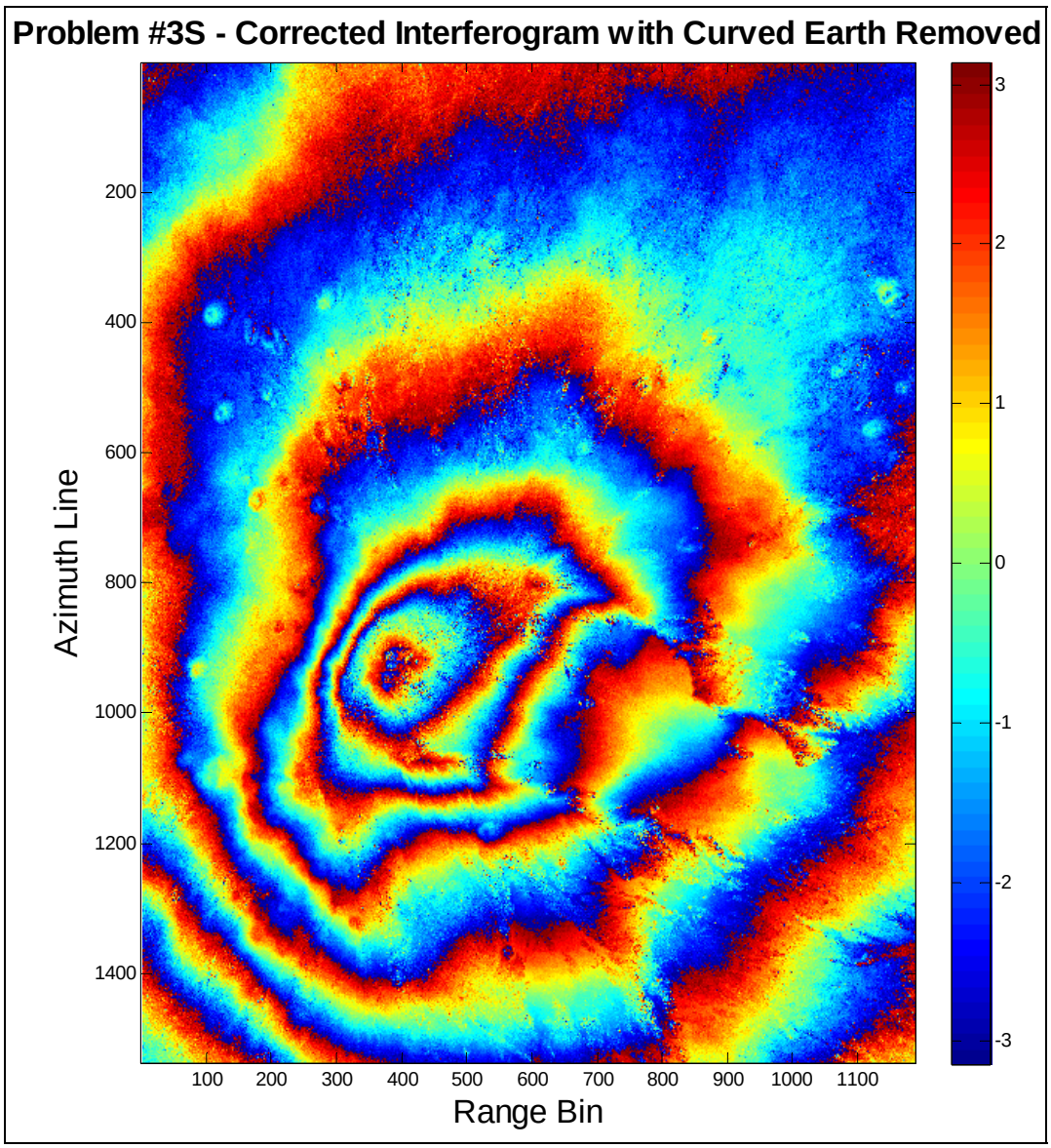

As we discovered when observing the curved earth fringe pattern, the corrections that we make to the flat earth fringe pattern by varying the height along the azimuth merely slant the fringes of constant phase, so the resulting interferogram with curved earth removed unsurprisingly looks nearly identical to the interferogram that we formed from subtracting the flat earth model.

Problem #4 – Ambiguity Height

Depending on where we set our reference range (or, equivalently, our reference angle), the ambiguity height that results from this 2π phase periodicity will vary. The contours or fringes of constant phase will repeat after 2π radians of phase difference, so each fringe corresponds to a height difference (the **ambiguity height**) of

$$2\pi = -\frac{4\pi B}{\lambda r_{ref}}\left[\frac{\cos\alpha}{\tan\theta_{ref}} + \sin\alpha\right]dz$$

For a given reference range, our ambiguity height is approximately

$$dz = \frac{-\lambda r_{ref}}{2B\left[\frac{\cos\alpha}{\tan\theta_{ref}} + \sin\alpha\right]}$$

However, the height depends on the choice of r_{ref} and θ_{ref}, as we can visualize in a plot of dz vs. r_{ref}:

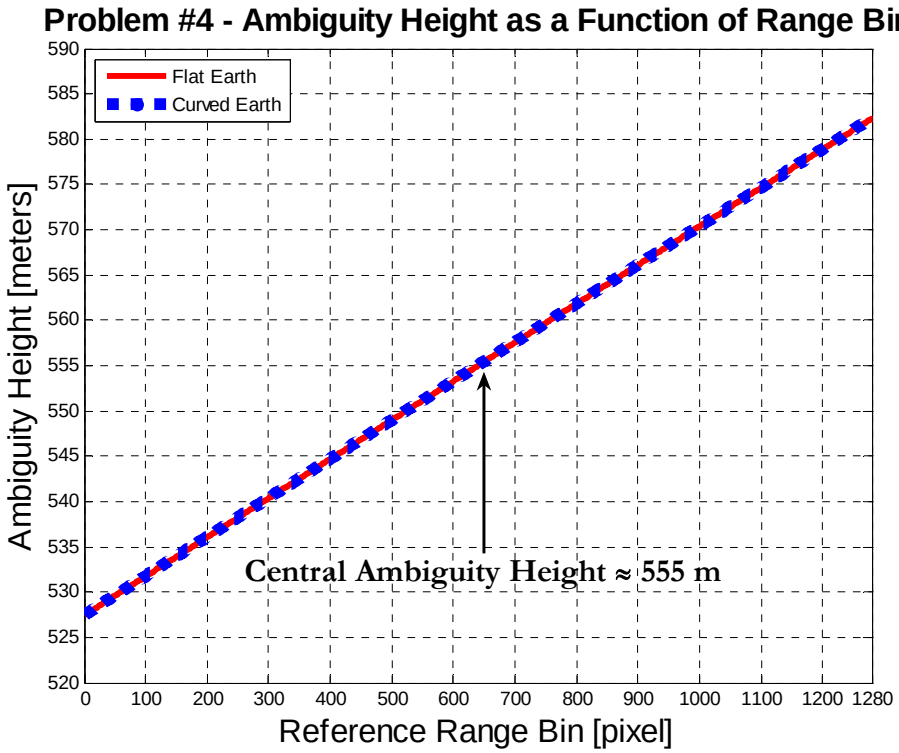

If we place our reference range at the central range bin (index 640), then the ambiguity height is approximately **554.966438 meters**. Nevertheless, complete topographic reduction requires inclusion of the range dependence, which we forego here. The curved earth ambiguity heights remain nearly exactly the same, since we consider only *deviations* in height; the absolute heights of the flat and curved earths differ, but, designating our reference altitude to be z_0 at the central azimuth line (line 768), the differential uncertainties dz do not.

Problem #5 – Phase Unwrapping

Unwrapping the flattened interferogram on the tree computers, we compress the number of data points but obtain both amplitude and unwrapped phase. Plotting the amplitude yields the reflectivity or brightness scale map that we have grown accustomed to viewing:

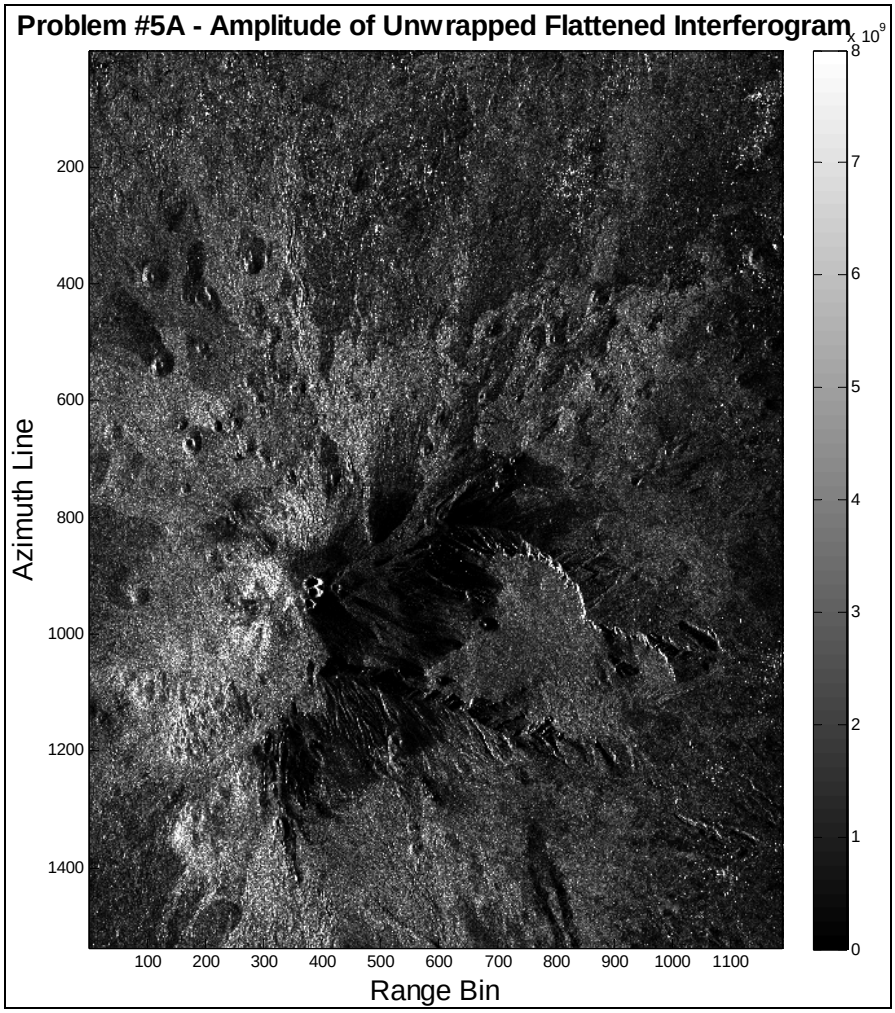

From the amplitude map, we observe several discrete point-like scattering targets reflecting especially well at the viewing geometry. The majority of the map is relatively dark in L-band, suggesting relatively flat terrain, whereas a set of points on the left side of Mt. Etna appears distinctly bright, possibly because of the material difference of the surrounding terrain. Mt. Etna is a particularly active strato volcano, so its ejecta – lava or landslides – could have roughened the left surface (relative to 24 cm wavelength) to yield high L-band reflectivity.

More importantly, however, we also obtain the unwrapped phase, which we will relate to elevation:

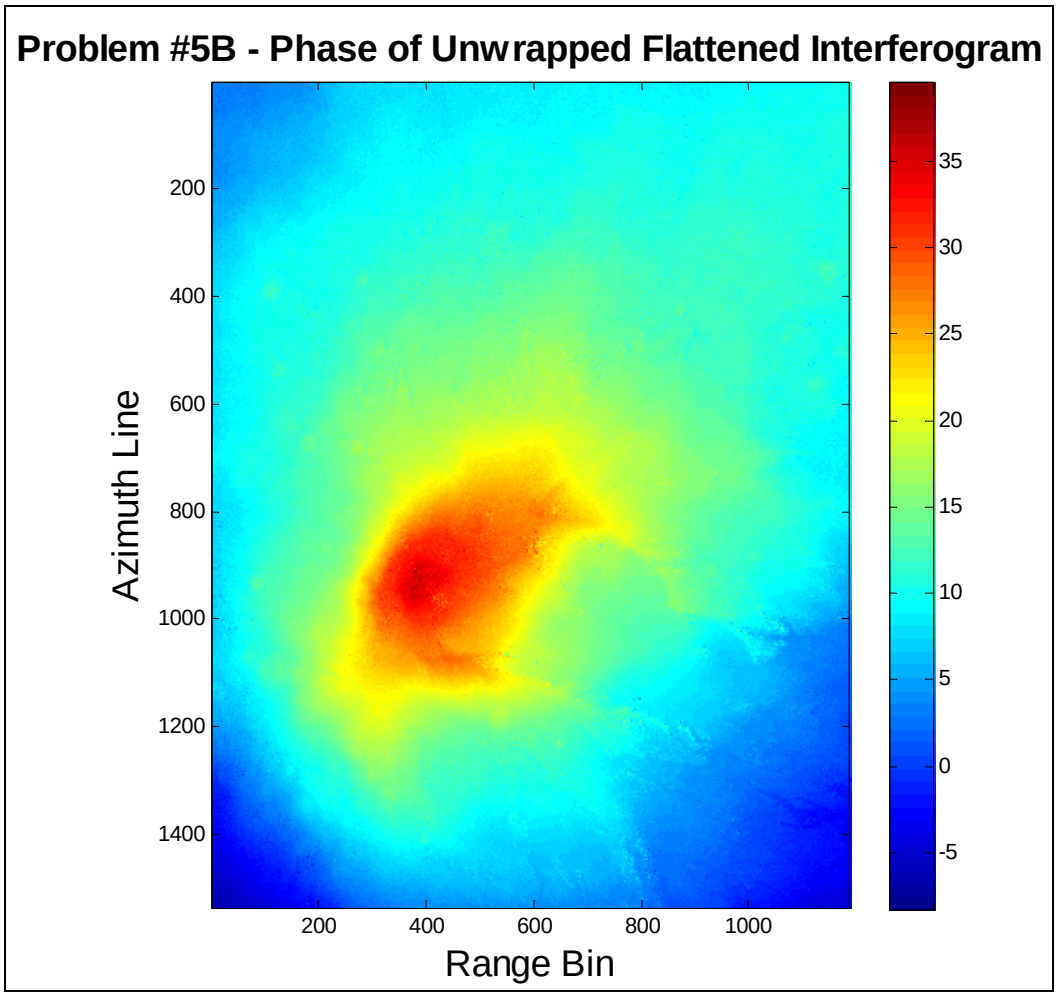

The unwrapped phase image begins to resemble a topographic elevation map, with the summit of Mt. Etna appearing reddish-orange due to its peak heights, and surrounding regions appearing progressively bluer to indicate lower heights closed to sea level.

Unwrapping the curved-earth approximation yields a similar result with slightly more contrast in the amplitude image:

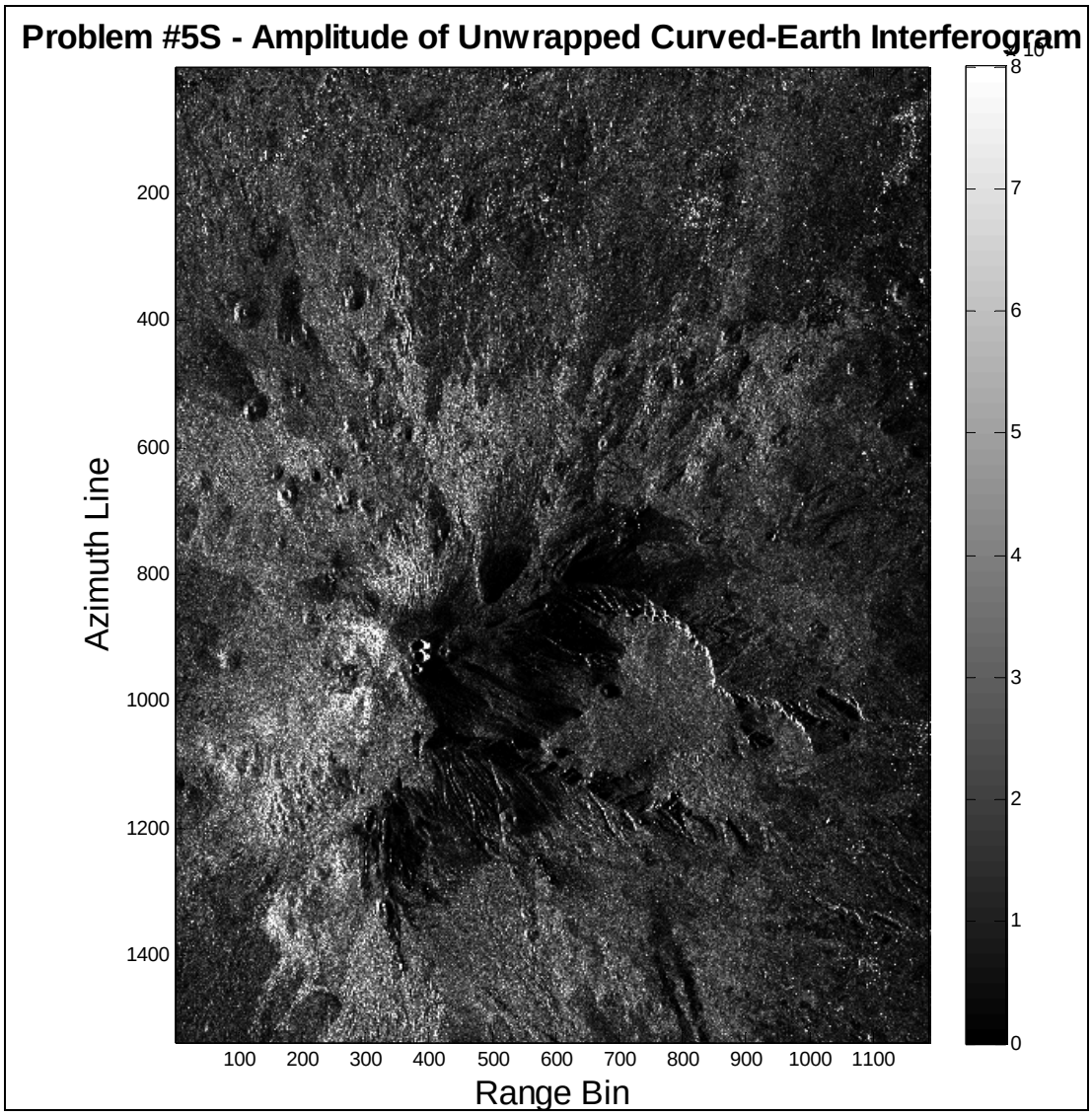

The finer speckles of the ground protrude slightly more prominently under the curved-earth assumption, renewing our hope that we have applied the more accurate model. The differences in detail are not earth-shattering, but we see enough small discrepancies – the white dots in the upper half of the image, the finer ridge lines, the more refined crater holes, and the slightly improved contrast – to know that our procedure has improved the image, if only marginally.

Likewise, we plot the unwrapped phase for the curved-earth approximation:

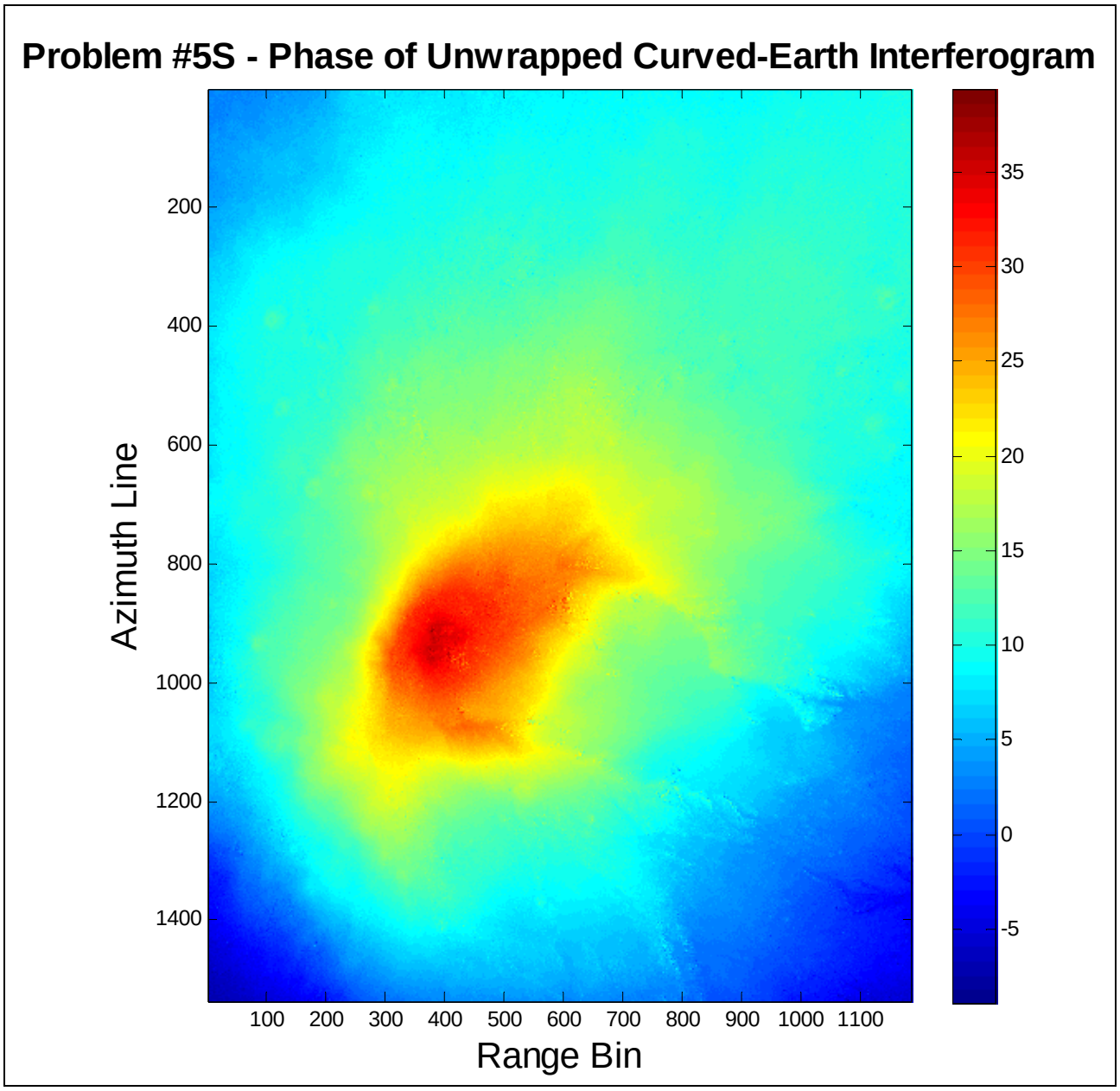

With such a flowing coalescence of colors on a two-dimensional image, it is difficult to perceive the effect of our curved earth assumption, but we shall see in our three-dimensional Digital Elevation Model (DEM) that the curvature we have considered is, indeed, subtly present.

Problem #6 – Digital Elevation Model (DEM)

In order to convert our unwrapped phase values into a model of surface height, we must normalize our scale by dividing by the phase periodicity 2π. Then, we build our entire elevation model around the single point of whose height we are certain; knowing that Mt. Etna has a peak height of 3350 m, we must ensure that our phase-normalized map has this maximum value. To scale all points accordingly, we subtract the current maximum from the map and add the known peak height of 3350 m, essentially forcing a shift of the imaged peak to the known peak height. Because we subtract and add the same standardization to each point, our resulting height model begins at 3350 m and scales down to lower elevations accordingly, with zero occurring at sea level due to normalization of the unwrapped phase. We set sea level at 0 m, and clip our image to [0 m, 3350 m] to obtain the Digital Elevation Model (DEM) pictured below:

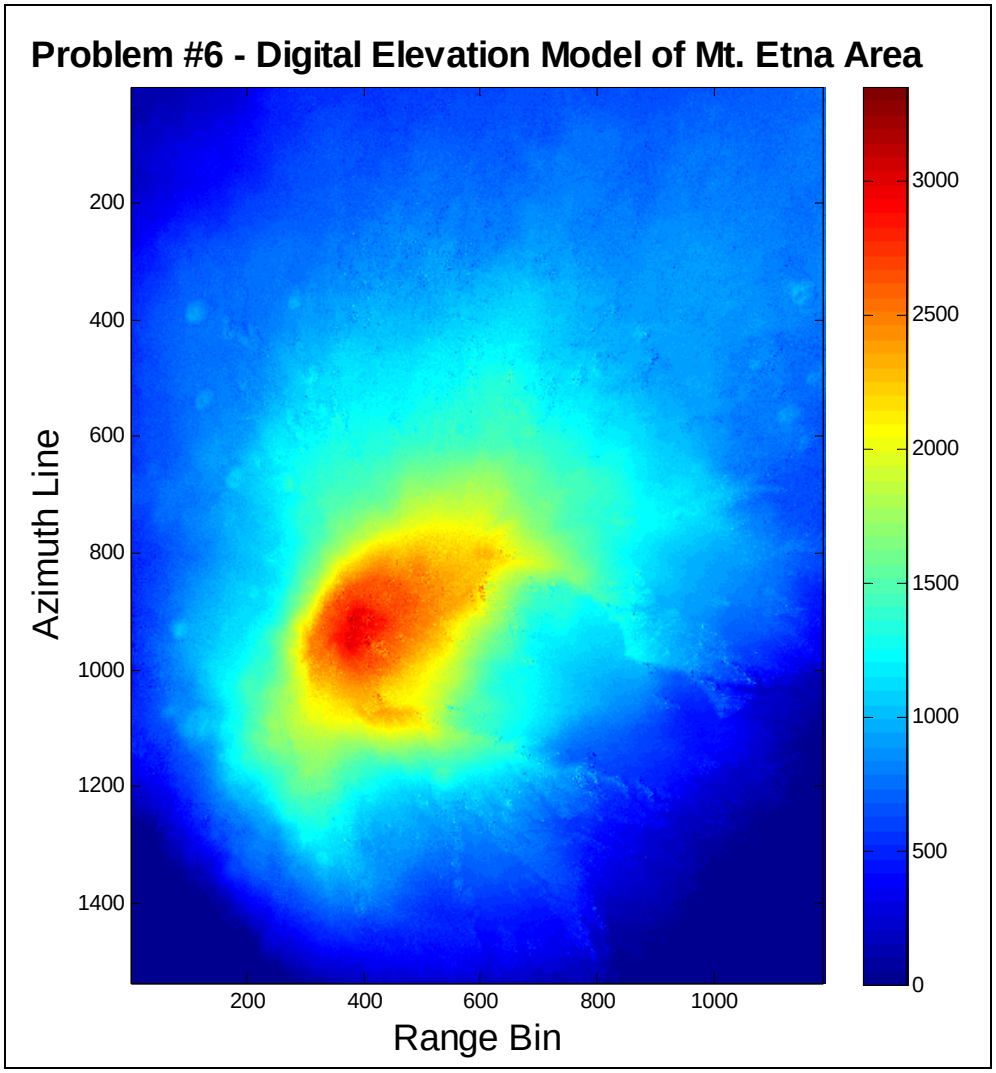

As desired, the peak of Mt. Etna appears as the maximum height (3350 m) in the image, with successively lower regions surrounding the peak appearing lower (more orange), all the way down to sea level at 0 m. Topographically, our DEM appears sensible considering the sloping surface around Mt. Etna. Because we began with the unwrapped phase, we are no longer sensitive to backscatter or point target brightness, allowing us to focus exclusively on the topographic height of our region. However, because the two dimensions (range and azimuth) still feature bin numbers, our DEM remains in radar coordinates.

We derive a similar DEM from the curved-earth model:

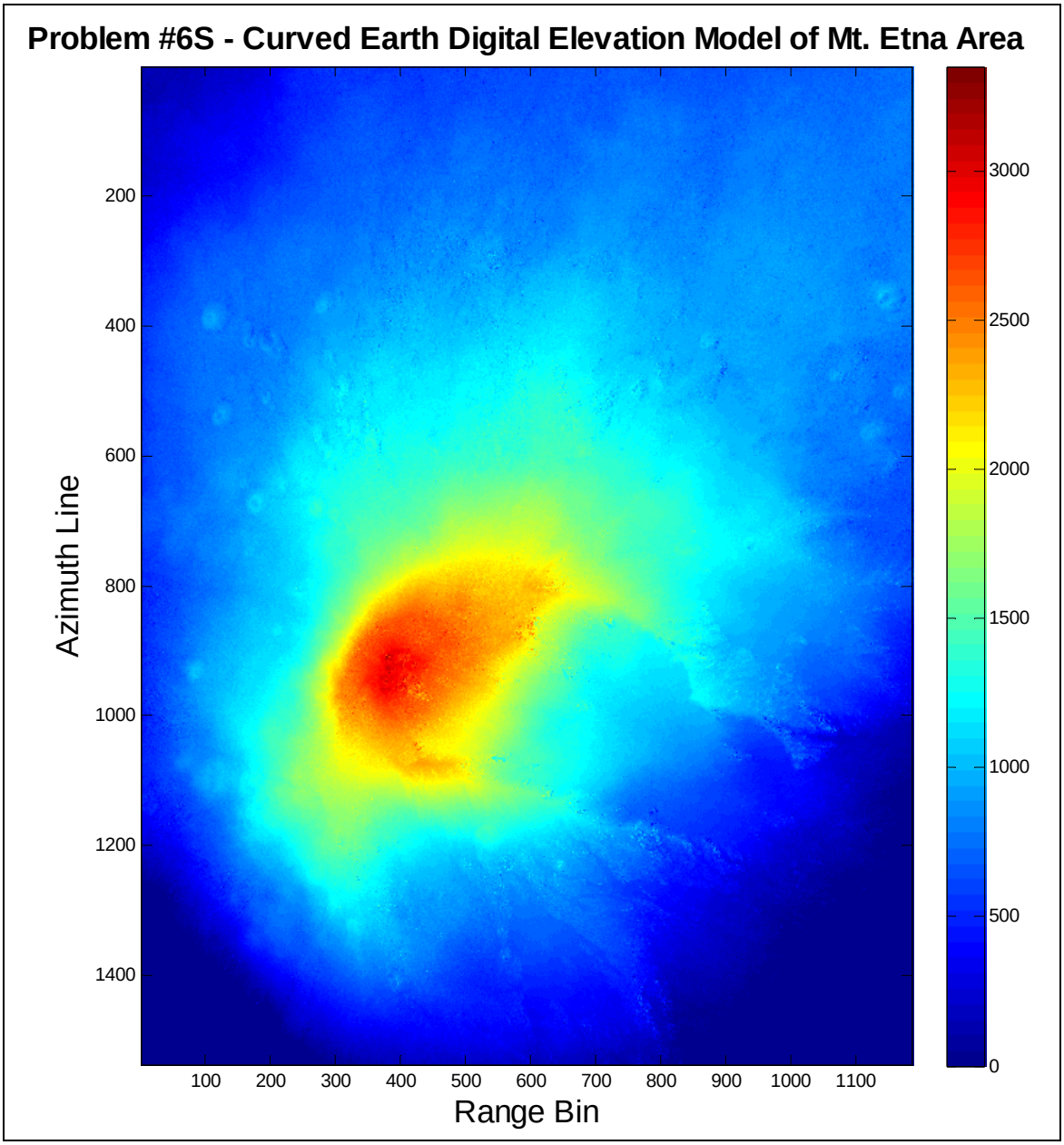

Problem #7 – Mapping Correlation into Height Error

Because the correlation offers a quantitative measure of our interferogram's accuracy in representing phase and hence range, we can use it also to quantify our digital elevation model's topographic height error, since we derived our DEM from the interferogram. Having already acquired the correlation map, we simply scale it according to the standard deviation relationship to obtain height error from phase error.

Assuming that our system operates with a high signal-to-noise ratio (SNR), and assuming that the correlations ρ collected in our map are predominantly thermal, we approximate topographic height error:

$$\sigma_z = \frac{\lambda r_{ref}}{4\pi B} \frac{sin\,\theta_{ref}}{cos(\theta_{ref} - \alpha)} \sqrt{\frac{1-\rho}{2\rho}}$$

Mapping correlations ρ to height errors σ_z for each point in our DEM, we obtain a standard deviation map:

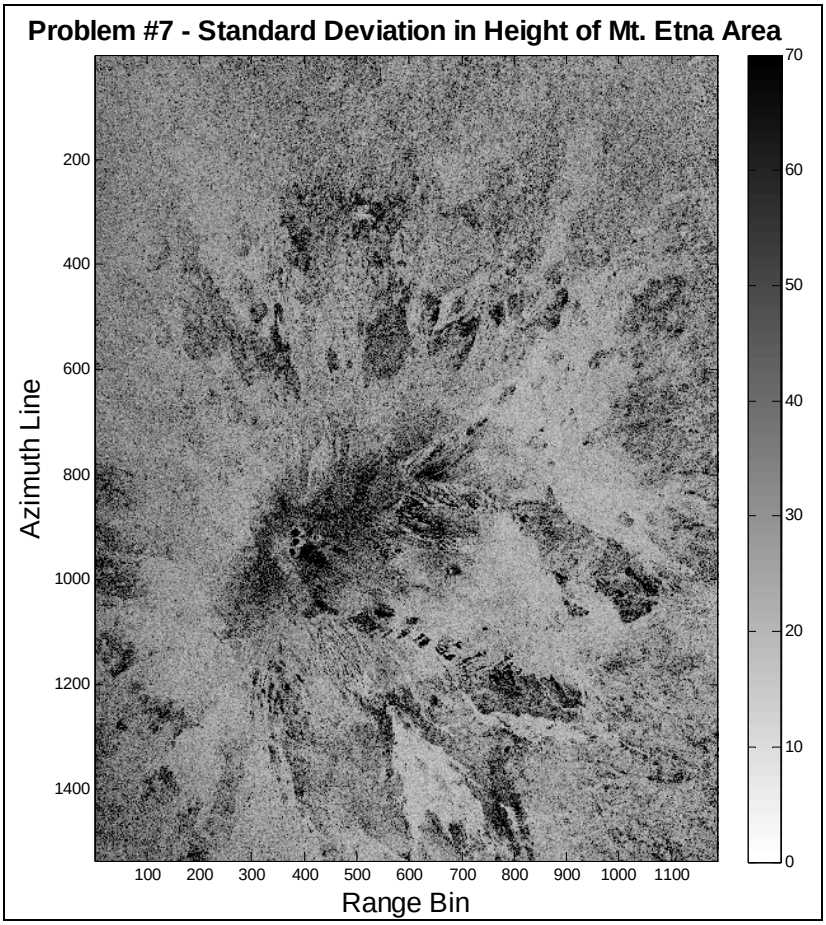

Even though the height error exceeds 70 m for several pixels, the mean error hovers around 36.52 m, which is tolerable for heights on the order of 3350 m. As we noted previously when compiling the correlation maps, the

most significant errors seem to occur on the mountain itself, where the slope is steepest and the heights largest. In fact, a side-to-side comparison of our amplitude map and this height error map reveals striking similarities:

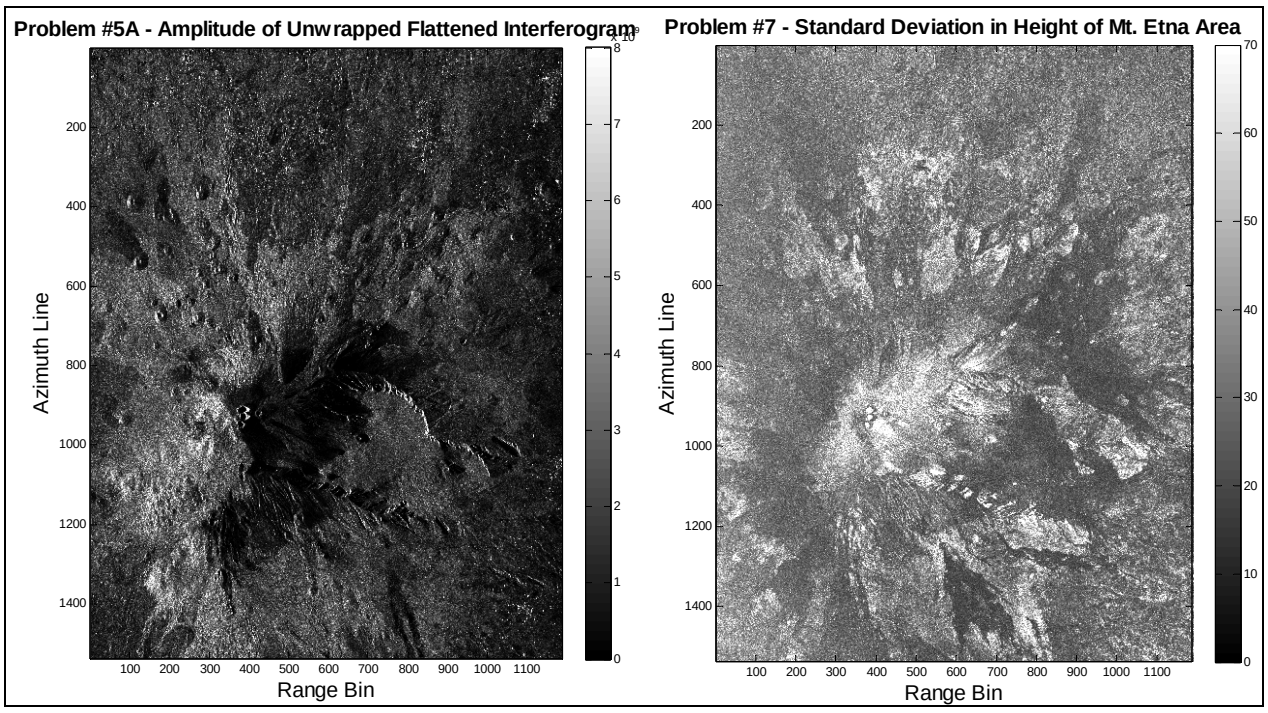

For example, the roughest locations with the highest frequency of ridges in the amplitude image appear with the greatest error in the standard deviation image; even the small crater-like holes appear distinctly in both images. Similarly, the flatter regions surrounding the mountain appear smooth not only in the amplitude image but also in the standard deviation image, where our height estimation error is minimal. Thus, based on correlation, our DEM provides seemingly accurate characterization of lower heights and flatter slopes in general, with steadily decreasing accuracy and increasing error as we ascend Mt. Etna and its numerous ridges. We attribute this error to the ambiguity height, as even small uncertainties in height begin to matter more as the height changes more quickly; as we ascend the steep slopes of Mt. Etna, it becomes more difficult to characterize the height accurately because it varies so rapidly.

On the other hand, our characterization of height error is incomplete; we assumed only thermal correlation, omitting spatial and temporal correlation from our calculation. Furthermore, we mapped errors from only phase noise, neglecting the typically smaller baseline noise and often-dominant orientation noise. Thus, to

obtain a definitive error model, we would have to consider these other forms of error and include spatial and temporal correlation.

For the curved earth problem, we cannot employ the flat-earth expression relating phase and height errors. Instead, we must re-derive the part of the relationship that assumes a flat earth:

$$\frac{\partial z}{\partial \phi} = \frac{\partial z}{\partial \theta} \cdot \frac{\partial \theta}{\partial \delta} \cdot \frac{\partial \delta}{\partial \phi}.$$

The expressions relating look angle and slant range difference remain the same:

$$\frac{\partial \theta}{\partial \delta} = -\frac{1}{B\cos(\theta - \alpha)}$$

$$\frac{\partial \delta}{\partial \phi} = -\frac{\lambda}{4\pi}$$

However, to relate the varying altitude with the look angle, we must now differentiate the Law of Cosines:

$$\cos\theta = -\frac{(R_{Earth} + z)^2 + r_{ref}^2 - R_{Earth}^2}{2 \cdot r_{ref} \cdot (R_{Earth} + z)}$$

$$\frac{\partial}{\partial \theta}[\cos\theta]\,\partial\theta = -\frac{\partial}{\partial z}\left[\frac{(R_{Earth} + z)^2 + r_{ref}^2 - R_{Earth}^2}{2 \cdot r_{ref} \cdot (R_{Earth} + z)}\right]\partial z$$

$$\frac{\partial z}{\partial \theta} = -\frac{2 \cdot r_{ref} \cdot [R_{Earth} + z(t)]^2 \cdot \sin\theta_{ref}}{[R_{Earth} + z(t)]^2 - r_{ref}^2 + R_{Earth}^2}$$

As a result of this slight correction, the standard deviation formula relating height and correlation also changes:

$$\frac{\partial z}{\partial \phi} = -\frac{\lambda \cdot r_{ref} \cdot [R_{Earth} + z(t)]^2 \cdot \sin\theta_{ref}}{2\pi B \cdot \cos(\theta - \alpha) \cdot [R_{Earth} + z(t)]^2 - r_{ref}^2 + R_{Earth}^2}$$

$$\sigma_z = \frac{\lambda r_{ref}}{4\pi B}\frac{sin\,\theta_{ref}}{cos(\theta_{ref} - \alpha)} \cdot \frac{2 \cdot [R_{Earth} + z(t)]^2}{[R_{Earth} + z(t)]^2 - r_{ref}^2 + R_{Earth}^2} \cdot \sqrt{\frac{1-\rho}{2\rho}}$$

Notice that the altitude $z(t)$ is no longer a simple constant, instead depending on the azimuth slow time coordinate, because our spacecraft no longer follows a straight-line trajectory but rather a circular one. Thus, in addition to changing our equation for computing the height error, we must also substitute a different azimuth-dependent height.

As before, we assume that our correlation is purely thermal, and we neglect baseline and orientation errors. Applying this new relation to the same correlation data, we obtain the image:

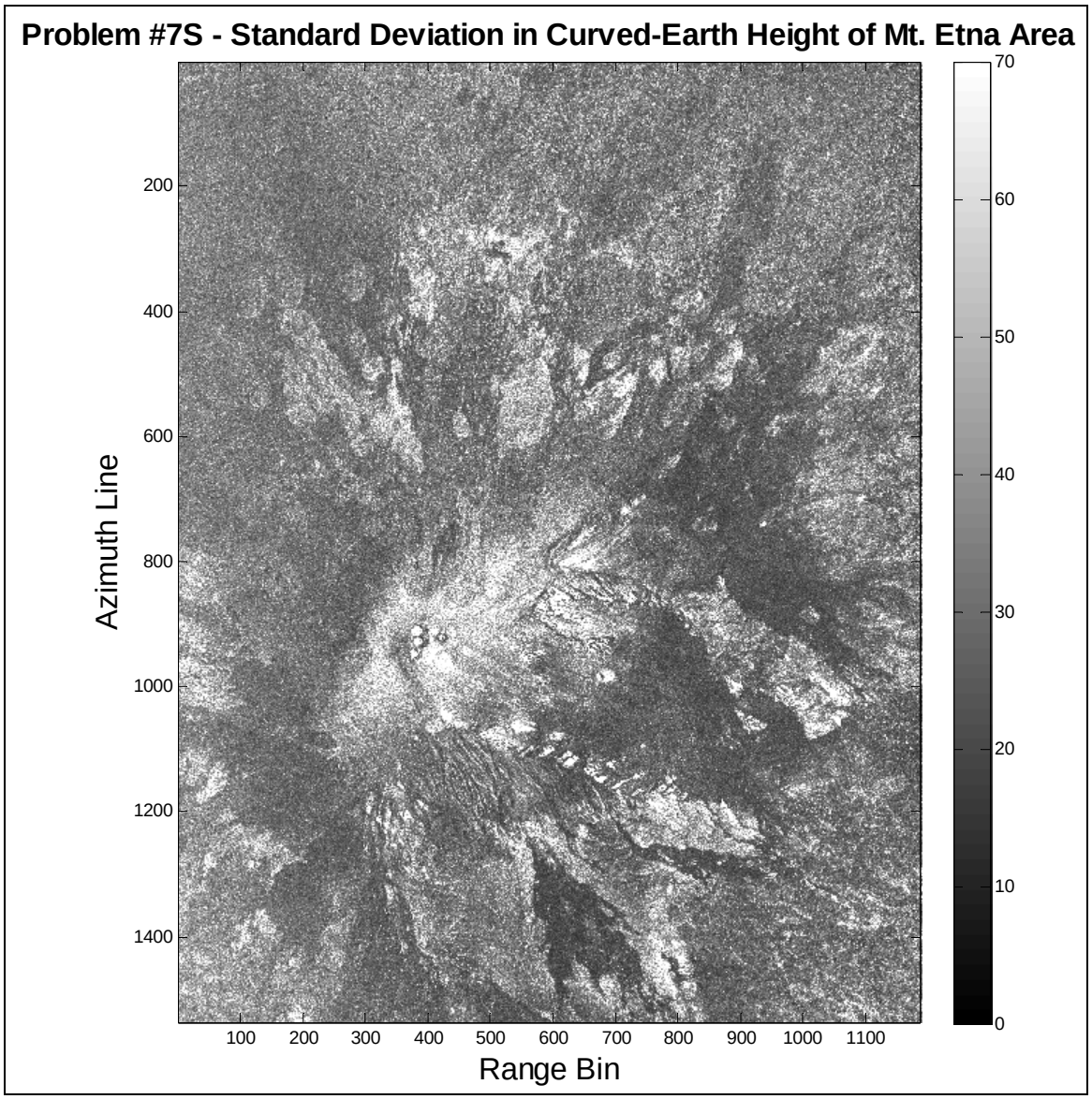

As expected, the changes are not visibly earth-shattering, as the mean height error still hovers around 37.7729 m (after the lines of useless junk data have been removed from the rightmost range bins). Thus, the curved earth approximation does not dramatically improve our height error estimate.

Problem #8 – Geocoding

Before we resample our image, we must convert from radar coordinates to ground coordinates in earth distances. To convert our slant range values into ground range coordinates, we compute

$$r_{ground} = \sqrt{r^2 - (z - h_{DEM})^2}$$

...or, in the case of a spherical (curved) earth, we project the central angle onto the surface of the earth:

$$r_{ground} = \beta \cdot R_{Earth} = cos^{-1}\left(\frac{(R_{Earth} + z)^2 + (R_{Earth} + h_{DEM})^2 - r^2}{2 \cdot (R_{Earth} + z) \cdot (R_{Earth} + h_{DEM})}\right) \cdot R_{Earth}$$

Along the azimuth direction, we apply the same ground pixel spacing as in range to obtain square pixels. Under the flat earth approximation, our first coordinate conversion from radar coordinates into the earth grid results in a perforated DEM, reflecting the fact that our resampling is non-linear; the mapping is not one-to-one:

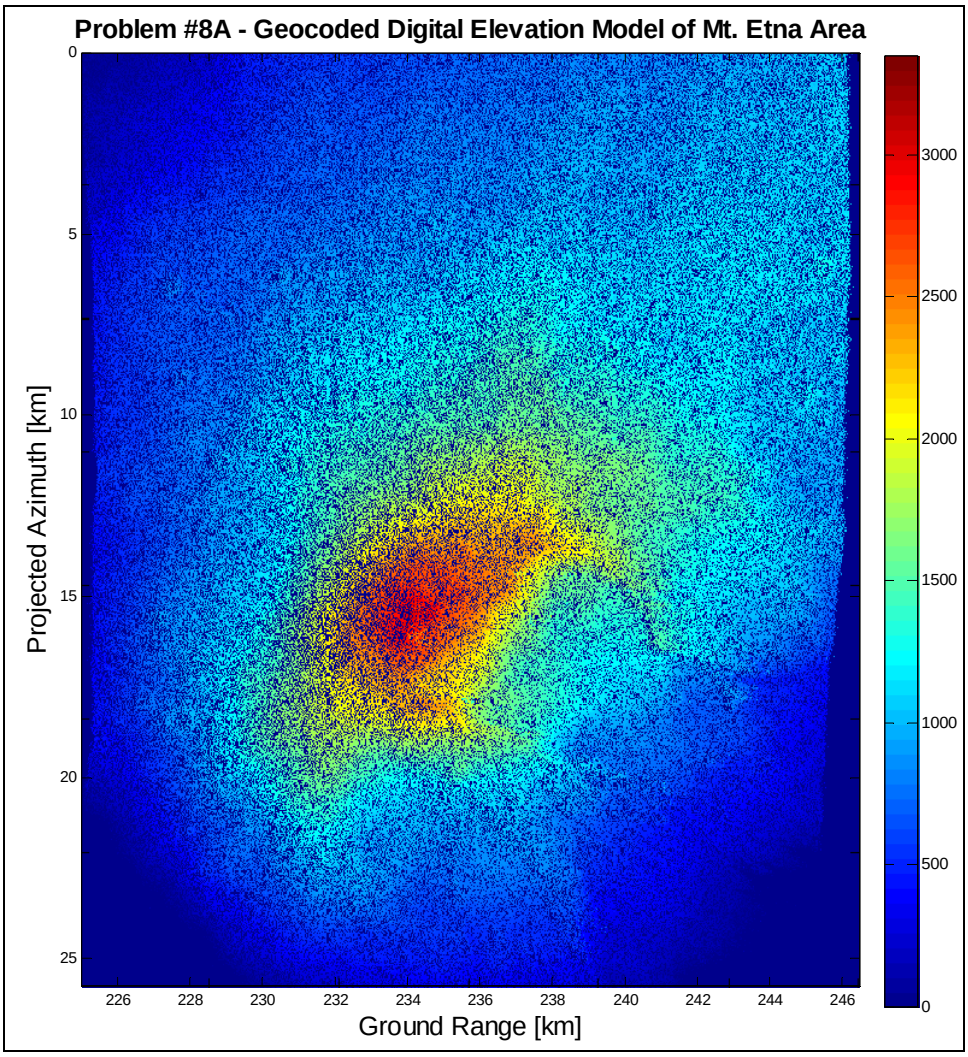

In order to fill the holes with reasonable pixel values, we can apply smoothening filters such as mean and median filters, or we can interpolate point-by-point. Filters are faster to apply than pointwise interpolation, but we can tap more sophisticated algorithms to produce more authentic images if we interpolate. For example, if we linearly interpolate each azimuth line, we compile the patched image:

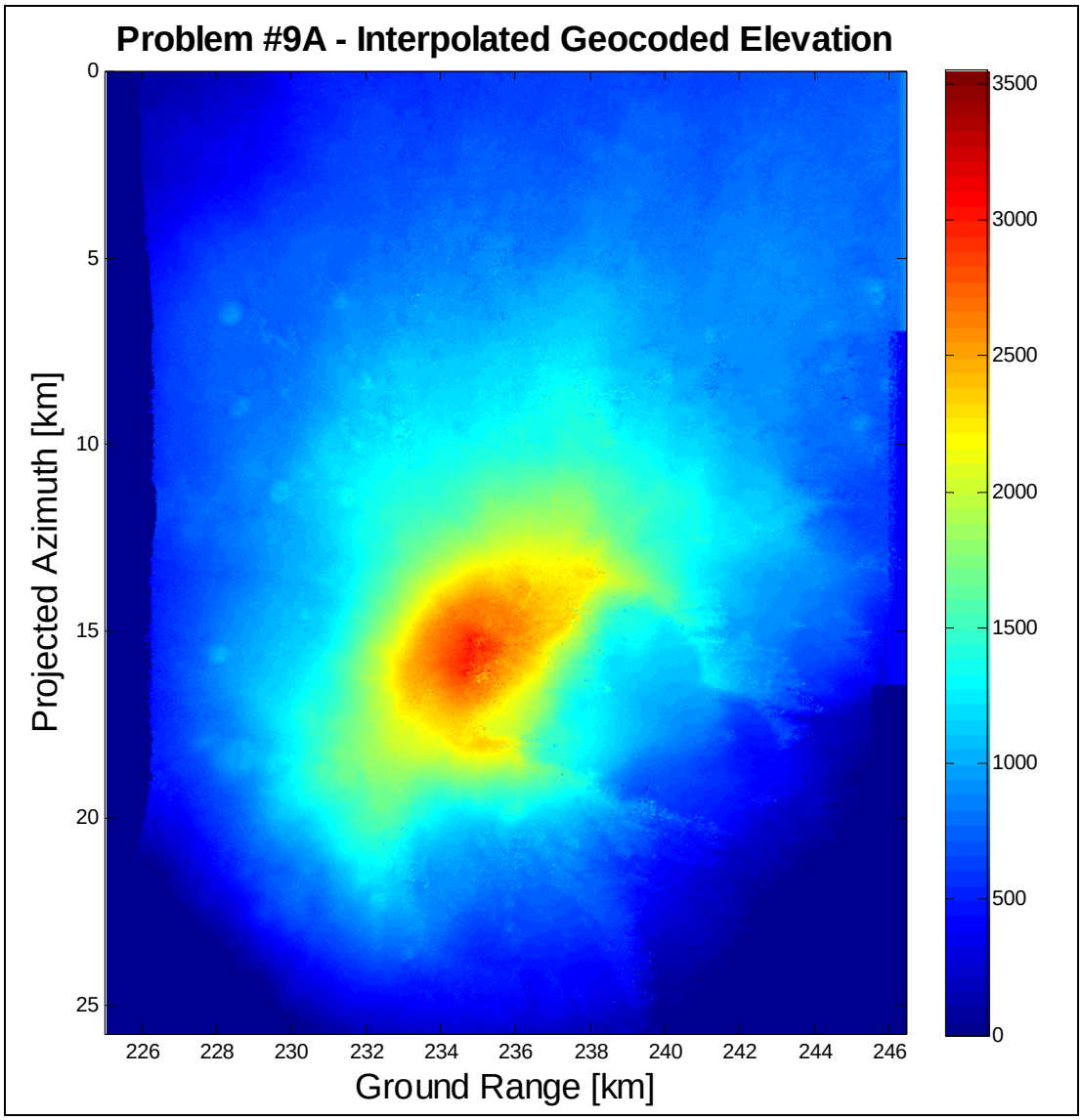

To check that our interpolation is valid, we might also plot the amplitude image with the same interpolation algorithm applied, leading to the visually intact display of surface brightness:

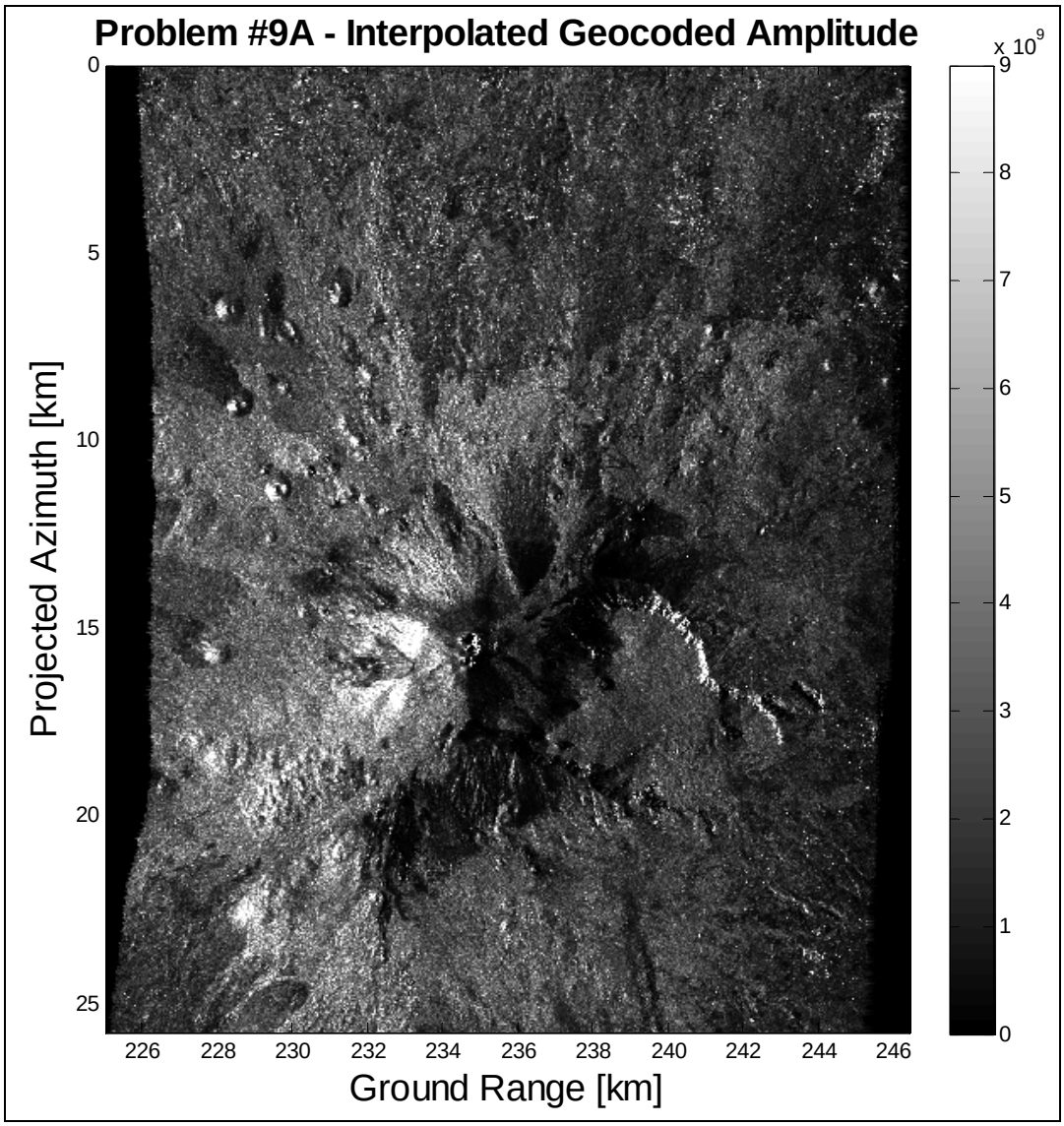

Since we can still recognize features in this amplitude image, we can rest assured that the interpolation properly patches the holes in the elevation image as well. Let us apply a median filter to the geocoded data to compare the effects, since median filters are typically more resistant to outliers (like the specks that we see) than both mean and interpolation filtering:

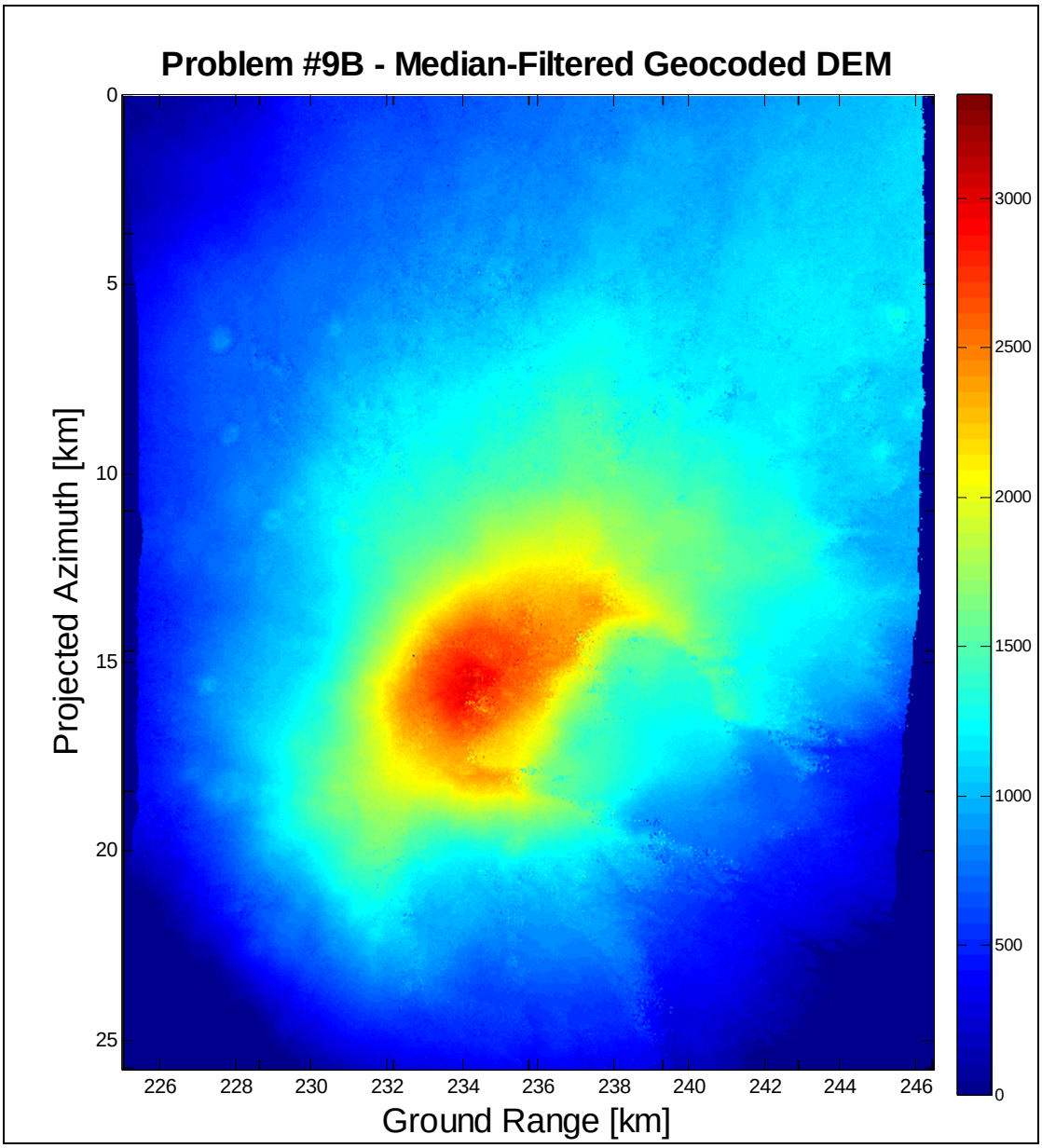

Compared to the linearly interpolated geocoded DEM, the median-filtered result retains more of the high-elevation points. However, at the same time, the upper-right corner of the image also appears at a slightly higher elevation, as the increased amount of blue suggests that the median filter obtains a generally higher elevation throughout the image, perhaps because the median is more resistant to low outliers that might weigh more heavily in the interpolation. Furthermore, the median filter works two-dimensionally, drawing points from several lines as opposed to linear one-dimensional line-by-line interpolation.

Finally, we expand our sinc interpolation to the spherical coordinate system, which we geocode using the central angle projection onto earth's curved surface. Applying the same algorithm, we obtain the geocoded DEM:

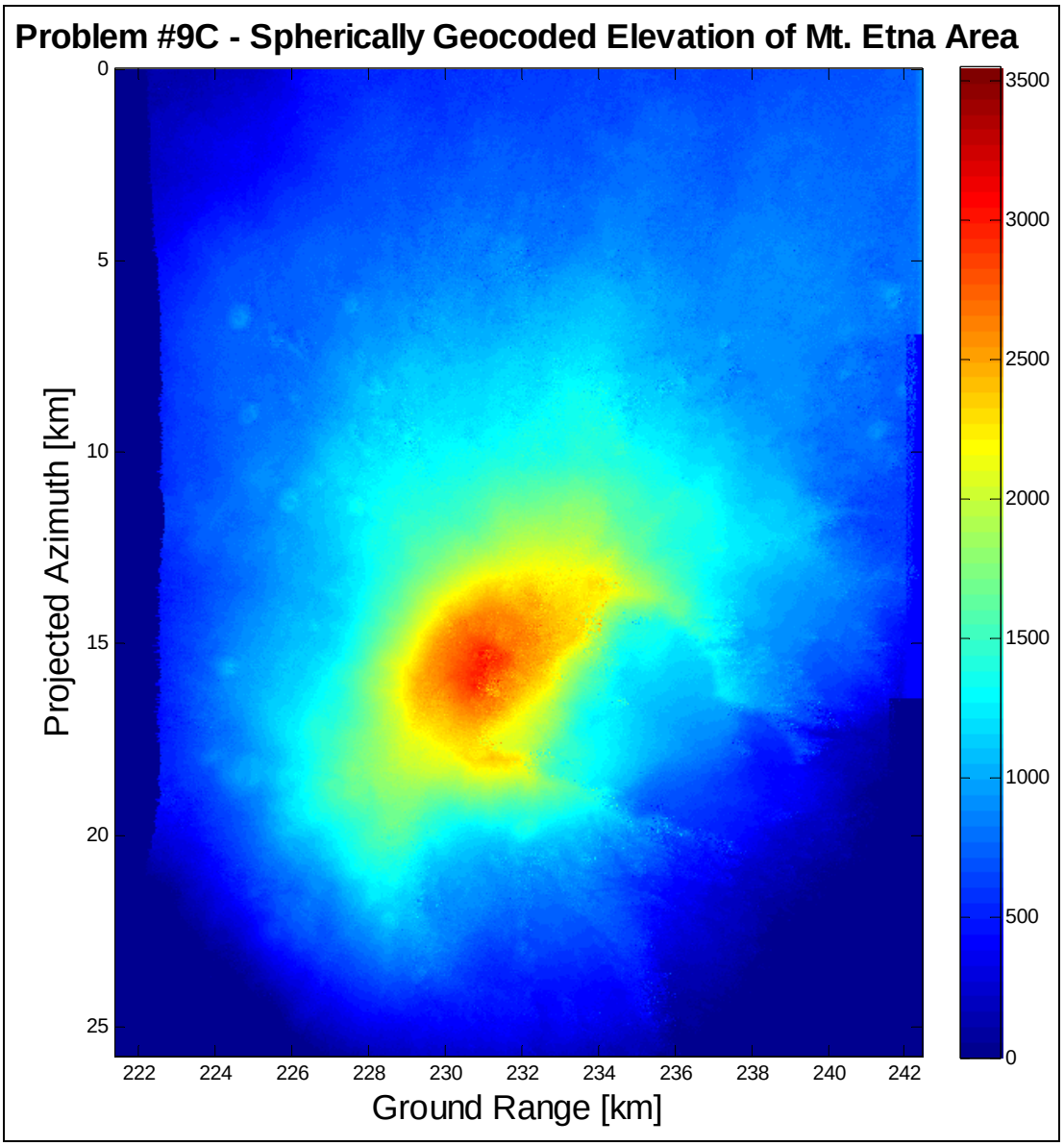

As we discovered in the interferogram, accounting for the slight curvature of earth offers little improvement over the flat earth approximation, but the consideration of even the slightest curvature – even if the consideration is not exact in its substitution of effective altitude – refines our DEM slightly, as we can ascertain in the interpolated amplitude image:

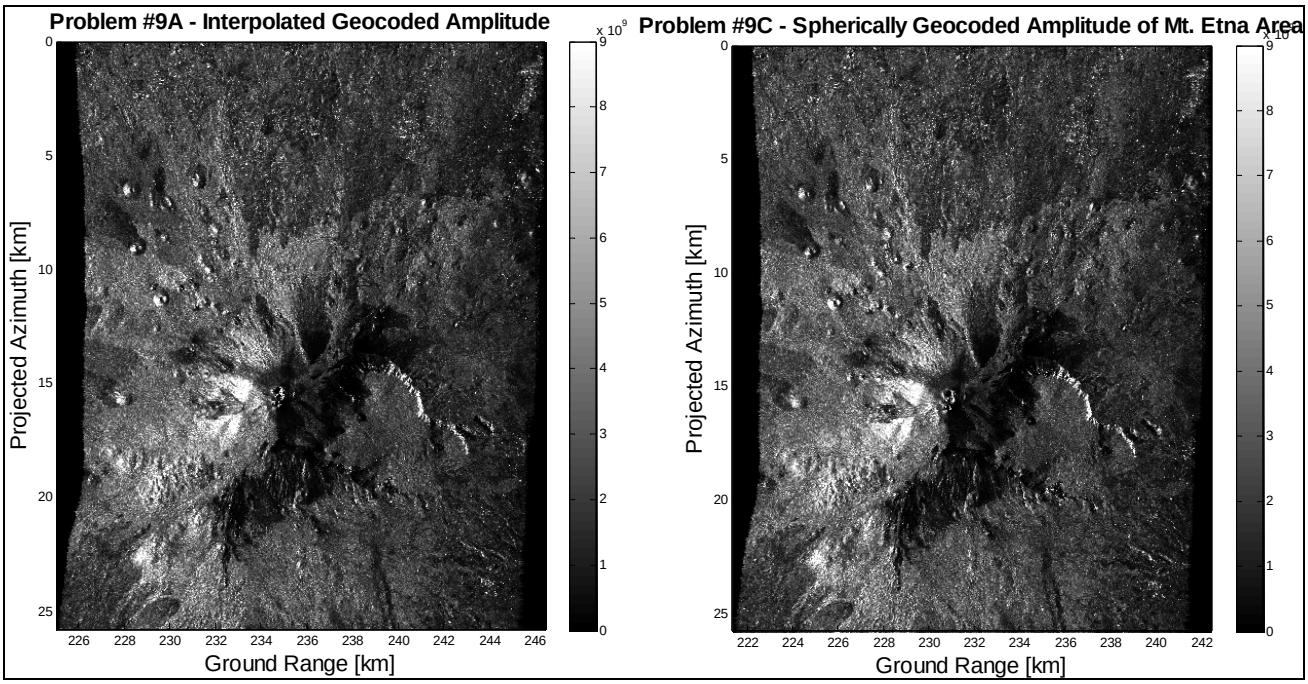

Once again, we consult the amplitude function to verify that our interpolation preserves geophysical sense, and the interpolation succeeds again, not only in patching the holes in our grid resampling but also maintaining order in the specific locations of features.

Finally, we can improve our geocoded DEM slightly with other finer techniques, such as two-dimensional interpolation, which yields the following image:

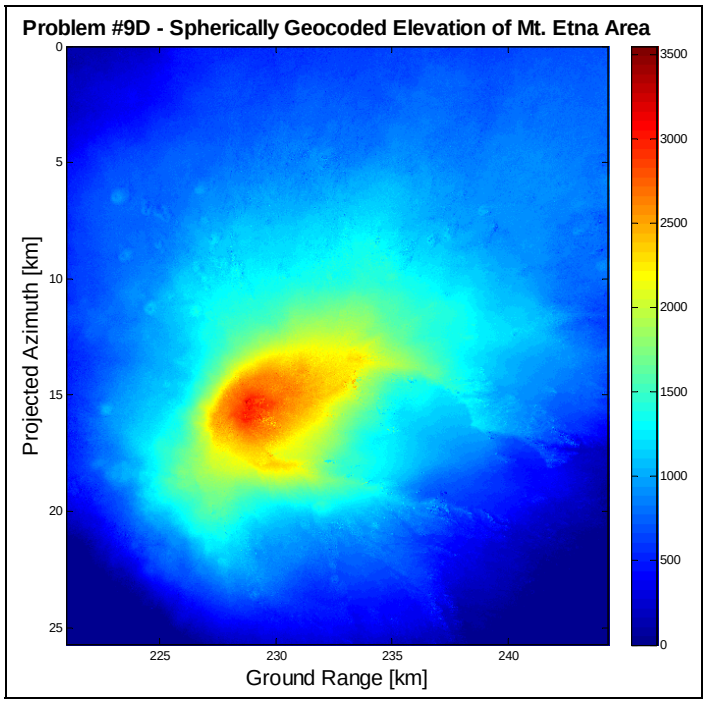

We can also apply different coloring schemes to accentuate the geography of Mt. Etna:

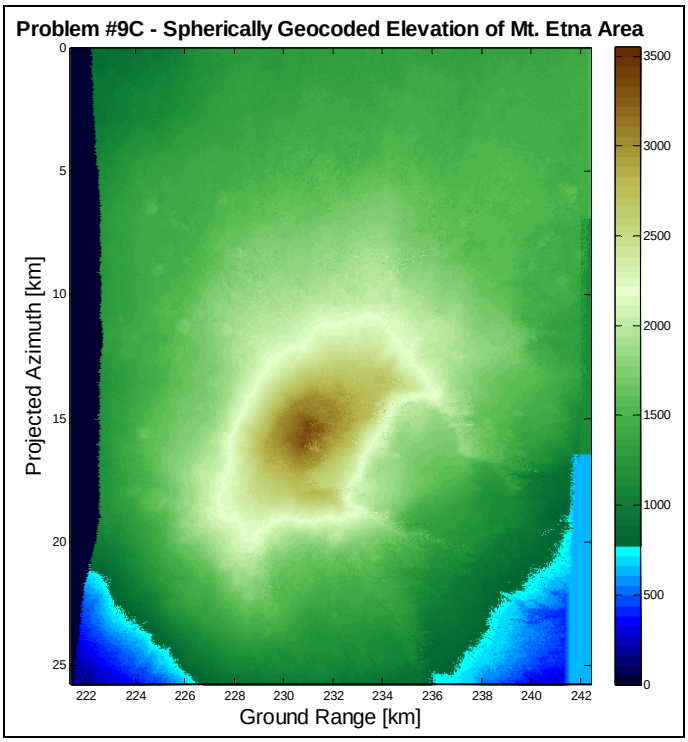

Last but certainly not least, we apply the curved-earth corrected to the range projection equations, thus refining the range and azimuth grid to reflect the slight curvature of our imaged region:

$$r_{ground} = \beta \cdot R_{Earth} = cos^{-1}\left(\frac{[R_{Earth} + z(t)]^2 + (R_{Earth} + h_{DEM})^2 - r^2}{2 \cdot [R_{Earth} + z(t)] \cdot (R_{Earth} + h_{DEM})}\right) \cdot R_{Earth}$$

Geocoding under this assumption, we obtain slightly corrected elevation and amplitude DEM plots:

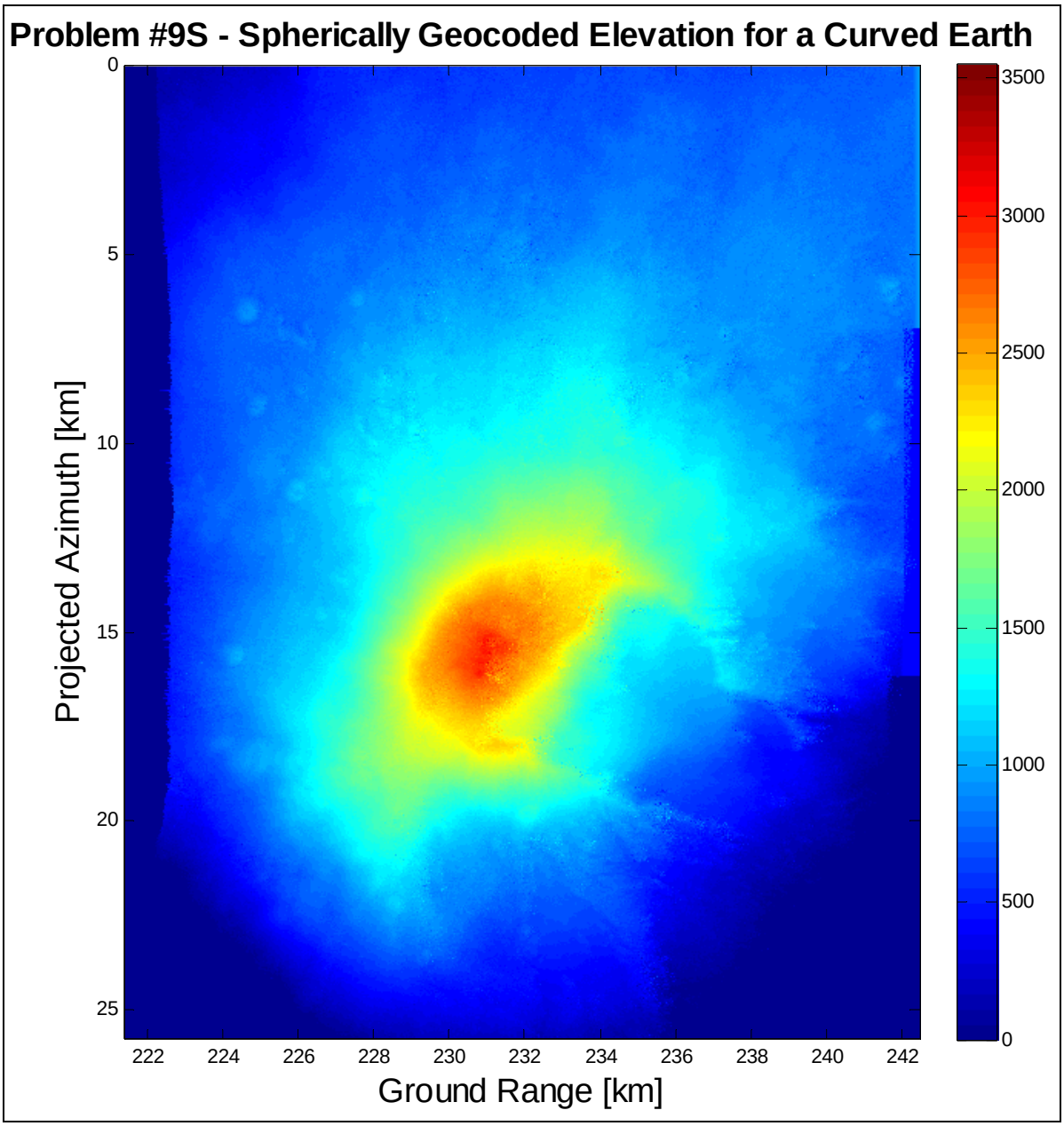

As verification, the amplitude tells us that we have interpolated correctly, as the features remain geographically intact with only slight degradation in the resolution due to linear interpolation:

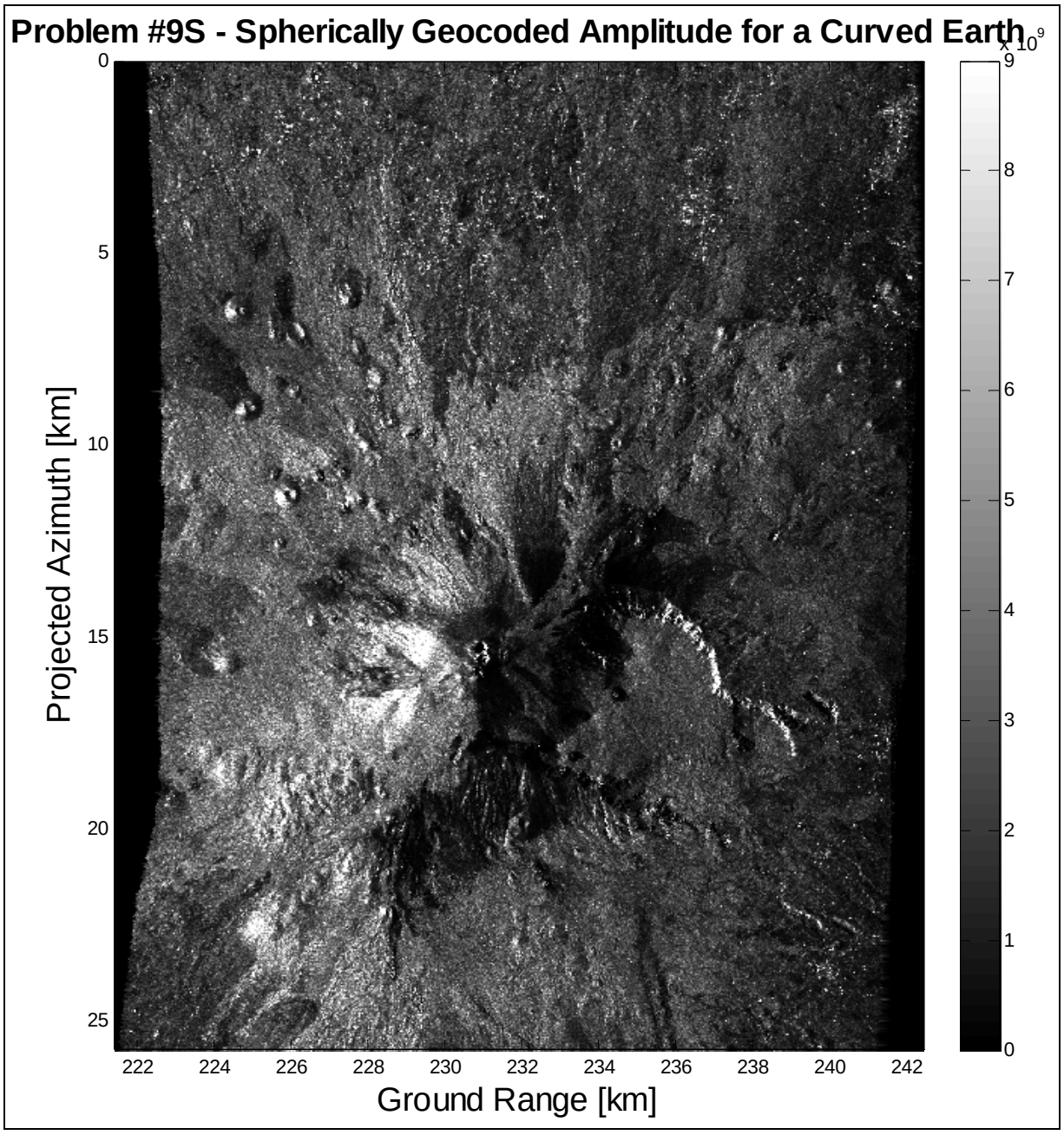

Though slightly blurred from our interpolation scheme, the brightness amplitude image still displays Mt. Etna in all her glory. As we noted previously, curved earth considerations round the surface appearance and accentuate details slightly more than the flat-earth image, but the difference is not otherwise noticeable. Finally, we construct a three-dimensional DEM:

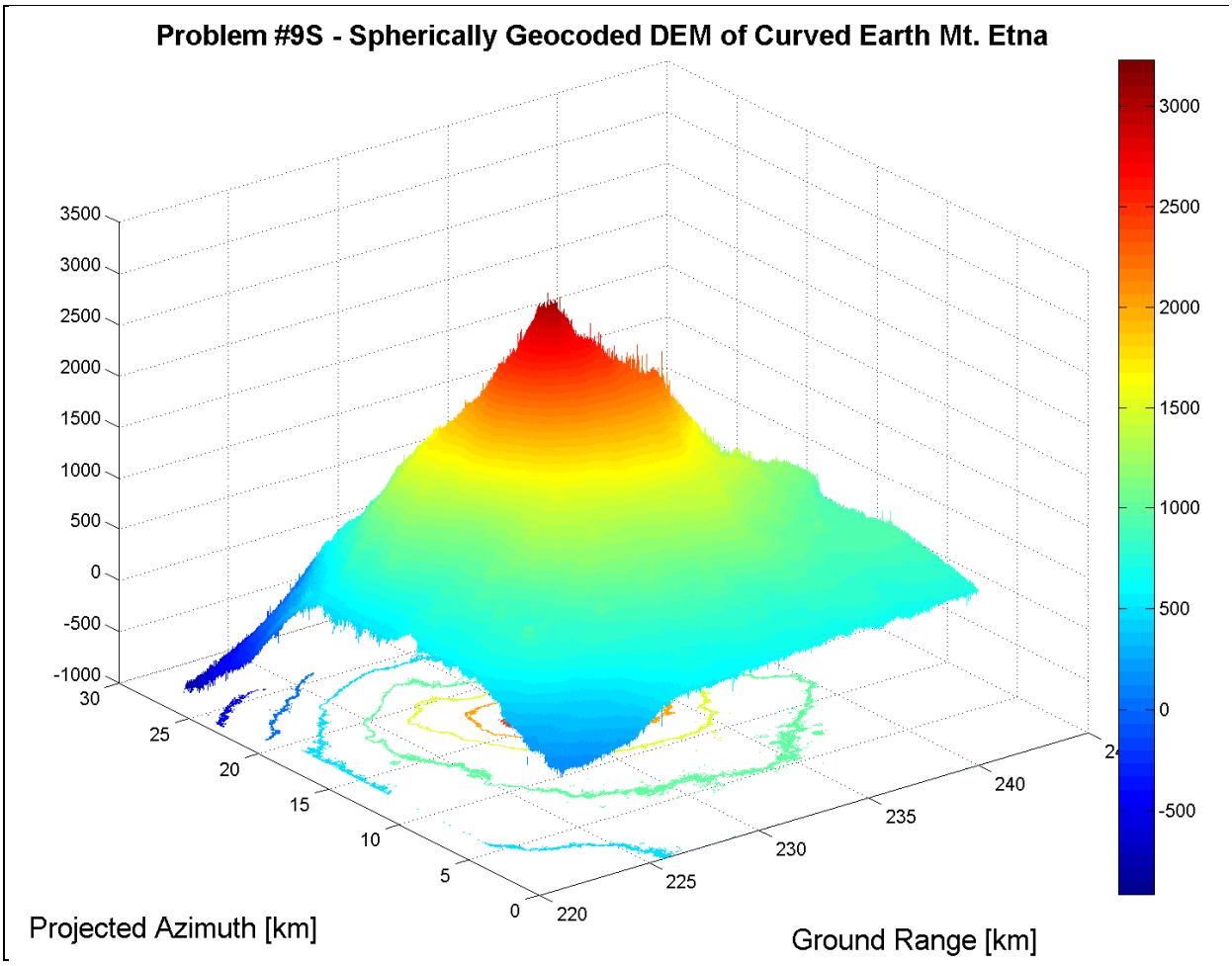

From this visual model of the surface near Mt. Etna, we perceive not only the steepness of the slope leading to the mountain's peak at 3350 m, but also the elliptical contour lines that display the ascent (or descent) in elevation. Even though our ambiguity height prevents us from assigning each pixel a definitive elevation above sea level, we can interpolate, both algorithmically and graphically, to produce such a surface.

Though the distinction may be difficult to perceive, we nevertheless concede that the curved-earth has introduced a slight curvature to our elevation model. The curvature is not extreme, because the earth is massive, and we have imaged but a small patch of it; nevertheless, we can see from the slightly bending shape of the surface – especially along the azimuth for a fixed range cross-section – that we have accounted for the slight curvature along the earth's surface. Most of this observed bending actually results from the physical topographic variation in elevation, but earth's spherical shape also contributes, if only slightly.

Please see hand-written notes for all curved earth derivations.